Dalton Transactions

RSC Publishing

PAPER

View Article Online
View Journal | View Issue

Cite this: *Dalton Trans.*, 2013, **42**, 16428

Oxidation state and covalency in f-element metallocenes (M = Ce, Th, Pu): a combined CASSCF and topological study†

Andrew Kerridge

CASSCF calculated wavefunctions are presented for three f-element metallocenes, $MCOT_2$ (M = Ce, Th, Pu; COT = η^8-C_8H_8). The configurational admixture of these systems is investigated and, where the $ThCOT_2$ ground state is well-defined as a monodeterminantal Th(IV) state, the cerocene ground state is found to be strong multiconfigurational and to bear strong similarities to that of plutonocene. Associated electronic densities are studied using QTAIM topological analysis and compared to CASSCF-derived densities of the aromatic systems benzene and the COT dianion. This analysis provides evidence of enhanced covalent character in plutonocene, supporting structural data calculated previously. Evidence of charge localisation in found in cerocene, this being most pronounced in its excited state of A_g symmetry. QTAIM analysis reveals that the ligand electronic structure is very similar in all metallocenes, and density differences show little variation in the ligand between the cerocene ground and excited state. Orbital contributions to integrated QTAIM properties are considered, and excellent agreement with experimentally determined f-orbital occupation is obtained. All methods of analysis support a Ce(IV) or mixed valence assignment of the cerocene ground state, whereas the A_g excited state is best described as a Ce(III) state.

Received 20th August 2013,
Accepted 19th September 2013

DOI: 10.1039/c3dt52279b

www.rsc.org/dalton

Introduction

Metal–ligand covalency is difficult to quantify in complexes containing open shell ions,[1,2] with traditional views based on the mixing of (near) degenerate orbitals failing in the presence of strong electron correlation. This (static) correlation manifests itself in the form of multiconfigurational character in the electronic wavefunction, and the independent particle approximation breaks down. The quantification of covalency is, however, of critical industrial importance. Current methods for the separation of minor actinides from lanthanides in spent nuclear fuel are based on the fact that the more radially extended 5f shell of the former results in enhanced covalent interactions with soft donor ligands[3] when compared to those of the latter, which are characterised by a contracted, core-like, 4f shell. The energetic stability afforded by this enhanced covalent interaction allows for the design of ligands which are strongly selective for actinides over lanthanides,[4,5] from which separation processes follow. The multiconfigurational character associated with such complexes can also result in ambiguity with regard to other chemical concepts, a prominent example being the assignment of oxidation state, as has been highlighted in the case of cerocene ($CeCOT_2$; COT = η^8-C_8H_8). Cerocene has, since its original preparation,[6,7] proved a controversial complex. Streitwieser *et al.*, based on photoelectron spectroscopy, concluded that cerocene was a Ce(IV) complex,[7] a view supported by atomic radii arguments[8] and electrochemical studies.[9] XANES studies,[10] however, provide evidence for a formal trivalent oxidation state, albeit with the caveat that 'formally Ce(IV) systems generally are strongly mixed valent'. It has also been concluded that substituted cerocene complexes should be classified as formally trivalent, based on XANES data.[11] Theoretical studies are also in disagreement: whereas Dolg and co-workers have shown though multiconfigurational self-consistent-field (MCSCF) studies that cerocene is dominated (~80%) by a Ce(III) configuration,[12] Kerridge *et al.* have performed complete-active-space self-consistent field calculations which show that that the Ce(III) configuration has a significantly reduced weighting,[13] concluding that the 'transfer of electron density from ligand to metal through occupation of bonding orbitals allows measures of the effective oxidation state [of Ce] to be lower than the formal +4 value, and indeed closer to +3'. Kaltsoyannis and co-workers have also shown that the related complex $CePn_2$ (Pn = η^8-C_8H_6), as well as $CeCp_3^+$ (Cp = η^5-C_5H_5), can be

Department of Chemistry, University College London, 20 Gordon Street, London, WC1H 0AJ, UK. E-mail: a.kerridge@ucl.ac.uk

†Electronic supplementary information (ESI) available. See DOI: 10.1039/c3dt52279b

characterised in a similar manner.[14,15] In contrast, there is a strong consensus regarding the tetravalent oxidation state of the actinide analogue thorocene ($ThCOT_2$),[16,17] whilst Kerridge and Kaltsoyannis have found similarities with cerocene in the multiconfigurational character of formally tetravalent plutonocene ($PuCOT_2$).[17] This is of particular interest since, with its similar ionic radius (r_{ion}(Ce(IV)) = 87 pm, r_{ion}(Pu(IV)) = 86 pm for hexacoordinated species), cerium is often used as an analogue of the highly radioactive plutonium in experimental studies of the immobilisation of spent nuclear fuel.[18]

In the present contribution, the electronic structure of $MCOT_2$ (M = Ce, Th, Pu), calculated using the CASSCF methodology, is analysed in terms of a natural orbital decomposition of the electron density.[19] These results give context for topological analysis of the electron density, employing the quantum theory of atoms in molecules (QTAIM).[20] It is intended that this electron density-based approach will remove the ambiguity inherently present in previous orbital-based studies. The study focusses on properties of both the central ion and the ligand, with particular attention paid to the degree of electron delocalization within the ligated COT ring, where comparisons are made to the prototypical aromatic system benzene, as well as the COT dianion. For the first time, integrated QTAIM properties are decomposed into orbital contributions in order to compare f-electron occupations to experimentally determined values.

Computational details

Complete-active-space self-consistent-field (CASSCF)[21] calculations were performed using version 7.6 of the MOLCAS quantum-chemical software package.[22,23] Throughout, ANO-RCC basis sets of polarised triple-zeta quality were used.[24–26] In order to investigate the effect of molecular structure, CASSCF calculations were performed at two different geometries: the previously derived CASPT2 (complete active space second order perturbation theory)[27] optimised-geometries,[13,17] and geometries obtained from density functional theory (DFT)[28,29] calculations, employing the popular B3LYP exchange correlation functional.[30,31] The latter geometries were obtained using the TURBOMOLE quantum-chemical software package,[32] employing the Ahlrichs basis sets[33] of polarised triple-zeta quality: def2-TZVP (Ce, C, H) and def-TZVP (Th, Pu). For Ce, Th and Pu, core electrons (28 for Ce; 60 for Th, Pu) were replaced with small-core relativistic effective core potentials.[34,35] Topological analysis was performed using the AIMAll[36] and Multiwfn[37] codes. Whilst all complexes in this study possess D_{8h} point group symmetry, restrictions of the MOLCAS code require that calculations were performed using its highest abelian subgroup, D_{2h}. Bearing this in mind, irreducible representations (irreps) of D_{2h} will be used in the discussion.

The reader's attention is drawn to the fact that the effects of dynamical correlation and spin–orbit coupling are neglected in this study. Whilst the former could be included *via* multiconfigurational second-order perturbation theory (*e.g.* CASPT2) and the latter *via* the restricted-active space state interaction (RASSI) approach, it was not possible to generate total electron densities in a manner amenable to QTAIM analysis. Inclusion of these effects would not be expected to significantly affect the results presented here, since the important correlation effects associated with the bonding interactions between ion and ligand are treated explicitly within the active spaces employed in this study. Furthermore, it has previously been shown[17] that the inclusion of spin–orbit coupling has virtually no effect on the calculated geometry of $PuCOT_2$, implying little change in the character of the bonding interaction. Preliminary QTAIM calculations were performed on the individual CASSCF states which comprise the RASSI-calculated spin–orbit coupled ground state of $PuCOT_2$ (namely the ^5A_g, $^5B_{2g}$ and $^5B_{3g}$ states; see ref. 17 for details) and only small differences were found. This is unsurprising since these CASSCF states only differ in the occupation of non-bonding 5f orbitals.

Active space definition

In all $MCOT_2$ calculations, a 16 orbital active space was constructed. This active space incorporates the highest occupied π-orbitals of a_u, b_{u1}, a_g and b_{1g} symmetry (in keeping with previous work[12,13,16,17]) along with the seven f-orbitals of a_u (f_δ), b_{1u} (f_σ, f_δ), b_{2u} (f_π, f_ϕ) and b_{3u} (f_π, f_ϕ) symmetry and the five d-orbitals of a_g (d_σ, d_δ), b_{1g} (d_δ), b_{2g} (d_π) and b_{3g} (d_π) symmetry. Adopting the CASSCF(n,m) notation to indicate a calculation incorporating an active space explicitly correlating n electrons in m orbitals, this selection results in CASSCF(8,16) calculations for $CeCOT_2$ and $ThCOT_2$, and CASSCF(12,16) calculations for the formally $5f^4$ $PuCOT_2$. C_6H_6 and $C_8H_8^{2-}$ calculations explicitly correlated all π-electrons, resulting in CASSCF(6,6) and CASSCF(8,10) calculations, respectively.

Results

DFT optimisations

Crystallographic data give separations between the central ion and the ring centroid of the COT ligand of 1.969 and 2.004 Å for $CeCOT_2$ and $ThCOT_2$, respectively.[16,38] Whilst no structural data exists for plutonocene, an approximate ion-centroid separation of 1.83 Å has been suggested, based on comparison of Th(IV) and Pu(IV) ionic radii.[17] Structural parameters resulting from B3LYP/def(2)-TZVP optimisation of the $MCOT_2$, C_6H_6 and $C_8H_8^{2-}$ systems are given in Table 1. As can be seen, B3LYP overestimates ion-centroid separations when compared to literature CASPT2 values, which themselves are in good agreement with crystallographic data. The closest agreement is found for $ThCOT_2$ (δr = 0.040 Å), followed by $CeCOT_2$ (δr = 0.047 Å) and $PuCOT_2$ (δr = 0.070 Å), although both methods predict a shortening of the ion-centroid separation when moving from Ce to Pu (Δr_{CASPT2} = 0.066 Å, Δr_{B3LYP} = 0.043 Å):

Table 1 Structural parameters of complexes considered in this study. r_{M-COT} represents the separation of the ion from the COT ring centroid

System	Method	r_{M-COT} (Å)	r_{C-C} (Å)	r_{C-H} (Å)	∠CCH (°)
$CeCOT_2$	B3LYP	2.011	1.408	1.084	175.4
	CASPT2[a]	1.964	1.404	1.087	180
$ThCOT_2$	B3LYP	2.055	1.410	1.085	175.4
	CASPT2[b]	2.015	1.404	1.087	180
$PuCOT_2$	B3LYP	1.968	1.409	1.084	175.4
	CASPT2[b]	1.898	1.404	1.087	180
COT^{2-}	B3LYP	—	1.414	1.097	180
C_6H_6	B3LYP	—	1.391	1.083	180

[a] ref. 13, [b] ref. 17.

given the previously discussed near-identical ionic radii of Ce(IV) and Pu(IV), the short Pu-centroid separation may be evidence of either increased covalency in the Pu–C bond, or increased electronic charge on the Ce centre, reducing the electrostatic interaction between ion and ligand. Attempts were made to stabilise a $\pi^3_{2u}4f^1_\delta$ ground state in cerocene through symmetry breaking, but in all cases, the resulting electronic state disobeyed the aufbau principle. DFT-optimised C–C and C–H bond lengths lie between those calculated for C_6H_6 and COT^{2-}, suggesting that the electronic structure of the ligated COT rings bears a strong resemblance to these aromatic systems.

CASSCF calculations

Analysis of the CASSCF-calculated electron structure of the $MCOT_2$ complexes begins with consideration of the natural orbitals (NOs)[19] and their occupations (NOOs) for each system. These are obtained *via* the diagonalisation of the first order reduced density matrix (RDM), and therefore provide an unambiguous orbital decomposition of the electron density. The NOs also have the property that they are maximum-occupancy orbitals and are thus a basis for the most compact CI description of the wavefunction. It follows that, for an electronic state constructed from a monodeterminantal wavefunction, every NOO will take a value of 0, 1 or 2. For a multiconfigurational electronic state, the deviation of the NOOs from integer values can be taken as a measure of multiconfigurational character[39] and, in the present study, can be related to the leading configurations in a given CASSCF-calculated electronic state. Fig. 1 compares the active space NOOs for the $MCOT_2$ systems considered here. Particular attention should be paid to the strongly occupied a_u/b_{1u} orbitals (of predominantly ligand π_{2u} character), along with the corresponding metal based a_u/b_{1u} f_δ orbitals. There are two reasons for focussing on these orbitals: firstly, they show the greatest deviation from integer occupations (no other active space orbitals exhibit deviation from integer occupation greater than 0.06) and secondly, the configurations corresponding to either a formal Ce(III) ($\pi^3_{2u}4f^1_\delta$) or Ce(IV) ($\pi^4_{2u}4f^0_\delta$) oxidation state differ in the occupations of these orbitals. Only NOOs calculated at the CASPT2 geometry are shown, deviations from these occupations at the B3LYP geometry are no greater than 0.02, and are typically much less. In the following discussion, all CASSCF states are expressed in terms of configurations of natural orbitals, and quantities obtained using B3LYP geometries are given in parentheses.

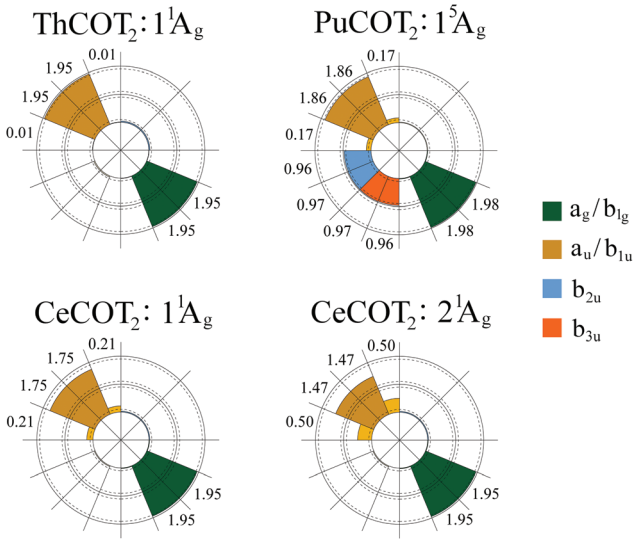

Fig. 1 Natural orbital occupations of $MCOT_2$ complexes, derived from CASSCF-calculated electron densities.

$ThCOT_2$: the ^1A_g ground state was calculated to be strongly monodeterminantal, and dominated by a $\pi^4_{2u}5f^0_\delta$ subconfiguration with a weight of 90.0% (89.8%), in agreement with previous studies.[13,16] Inspection of the NOOs shows that no occupation deviates from an integer value by more than 0.05. In particular, the occupation of the metal based a_u and b_{1u} $5f_\delta$ NOs is just 0.01 (0.01).

$PuCOT_2$: the ^5A_g ground state exhibits significant multiconfigurational character, manifested in the non-integer occupations of the a_u and b_{1u} NOs, including $5f_\delta$ NOOs of 0.17 (0.19). However, the state is still dominated by a $\pi^4_{2u}5f^2_\pi5f^2_\phi5f^0_\delta$ configuration with a weight of 74.4% (72.2%), with a 5.7% (6.7%) contribution from $\pi^3_{2u}5f^2_\pi5f^2_\phi5f^1_\delta$ configurations and a 3.4% (3.5%) contribution from $\pi^2_{2u}5f^2_\pi5f^2_\phi5f^2_\delta$. The reduction of 15.6% (17.6%) in the leading configuration when moving from thorocene to plutonocene reflects the energetic stabilisation of the 5f manifold as one moves across the actinide series, with the $5f_\delta$ components acting as correlating orbitals to the ligand based π_{2u} orbitals.

$CeCOT_2$: here both the ground and first excited states of ^1A_g symmetry are considered. As found previously,[13] the ground state, though strongly multiconfigurational, with NOOs bearing a strong resemblance to those of plutonocene, is predominantly comprised of a $\pi^4_{2u}4f^0_\delta$ configuration with a weighting of 58.5% (56.9%), with $\pi^3_{2u}4f^1_\delta$ contributions totalling 22.8% (24.2%) and $\pi^2_{2u}4f^2_\delta$ contributions of 8.5% (8.7%). This configurational admixture does not, therefore, support the assignment of a trivalent Ce oxidation state, but instead suggests strongly mixed-valence character. The excited 2 ^1A_g state, however, which lies 1.61 eV (1.54 eV) higher in energy at the CASPT2 level, is comprised of dominant $\pi^3_{2u}4f^1_\delta$ configurations with a weighting of 84.6% (84.6%), and $\pi^2_{2u}4f^2_\delta$

contributions totalling 6.2% (6.1%), and therefore appears consistent with a Ce(III) oxidation state. This assignment is further supported by the occupation numbers of the two components of the energetically degenerate $4f_\delta$ orbitals. Each component has a NOO of 0.50 (0.50), as would be expected for a trivalent complex.

Interpretation of oxidation state through configurational admixture can, however, lead to ambiguities. Unlike configuration interaction (CI) based approaches, multiconfigurational self-consistent-field (MCSCF) methods such as CASSCF incorporate orbital relaxation. This has previously been highlighted in the case of cerocene,[13] where configurational admixture was shown to be strongly dependent on the details of the calculation. This ambiguity finds its origin in the fact that the ligand- and metal-based a_u/b_{1u} orbitals can mix during the CASSCF calculation. The degree of this mixing varies, but can be balanced by the corresponding CI coefficients such that the total electron density remains constant. Fig. 3 shows the degree of mixing present between the ligand π_{2u} and metal f_δ orbitals in each complex studied here. Thorocene exhibits the smallest degree of hybridisation, as might be expected when considering the high energy of the 5f manifold (which lies above the $6d_\sigma$ orbital). plutonocene exhibits greater mixing due to the energetic stabilisation the 5f manifold, but cerocene shows the highest degree of mixing: taking maximally localised π_{2u} and $4f_\delta$ orbitals as (orthogonal) basis vectors, the $CeCOT_2$ NOs shown in Fig. 3 are obtained by rotation of one into the other through an angle of 0.28 rad (16°). Whilst some way short of the maximal mixing that would be obtained by a rotation though an angle of $\pi/4$ rad (45°), this still substantial mixing indicates the presence of low-lying $4f_\delta$ orbitals, while somewhat hampering the attempt to clarify the Ce oxidation state, since both the 'π_{2u}' and '$4f_\delta$' orbitals (occupations of which might be used to differentiate) exhibit significant metal contributions.

QTAIM: topological analysis

In order to better understand the details of the electronic structure of the $MCOT_2$ complexes, topological analysis of the electron density was carried out. This analysis employed the quantum theory of atoms in molecules (QTAIM),[20] which has previously been shown to be of great use in understanding covalency trends in the actinide series when applied to DFT-calculated densities.[2,40,41] QTAIM provides a method for the partitioning of the molecular electron density into a set of space filling open quantum systems[42] bound by surfaces satisfying the condition $\nabla\rho(\mathbf{r})\cdot\mathbf{n}(\mathbf{r}) = 0$: typically, each of these volumes, or basins, can be associated with an atom. The corresponding topological analysis gives a set of critical points, satisfying the condition $\nabla\rho(\mathbf{r}) = 0$. Of most interest here are the bond critical points (BCPs) between pairs of bonded atoms. These BCPs lie at the intersection of the bond path (the path of maximum electron density between the two atoms) with the interatomic surfaces. The value of the electron density at this point, along with its Laplacian, can be used to interpret the nature of the interactions. As a general rule, $\rho_{BCP} > 0.20$ a.u. and $\nabla^2\rho_{BCP} < 0$ for a covalent bond, whilst $\rho_{BCP} < 0.10$ a.u. and $\nabla^2\rho_{BCP} > 0$ indicates an ionic bond. More broadly, increasing values of ρ_{BCP} and reduction in $\nabla^2\rho_{BCP}$ indicate increasing covalent character and stronger bonding interactions. Fig. 4 show the molecular graphs of cerocene and the COT dianion (the corresponding thorocene and plutonocene graphs were omitted due to their qualitative similarity to that of cerocene). The absence of a compensating dicationic charge in the COT^{2-} system leads to the excess electronic charge adopting a somewhat diffuse character, and so, in order to give a more useful reference to the complexed COT ligand, CASSCF calculations were performed in the presence of a +2 point charge, located at the average ion-centroid separation of the metallocenes considered here (r = 1.959 Å). Throughout this contribution, all discussions regarding the COT dianion refer to this charge-compensated system. The differences in QTAIM properties between this and the uncompensated dianion are given in Table S1 of the ESI.†

BCP data for all systems considered in this study are presented in Table 2. Due to the strong similarity in results obtained from CASPT2- and B3LYP-optimised geometries, only the former are discussed here (results for the latter can be found in Table S2 of the ESI†). Table 2 shows that, of the metallocenes, plutonocene exhibits the largest value of ρ_{BCP}, and cerocene the smallest. Although by the criteria defined above all metal–carbon interactions here are best described as ionic in character, the increased value of ρ_{BCP} in $PuCOT_2$ can be explained by considering the contribution of f-orbitals to the bonding. In the lanthanides, the 4f shell is highly contracted, and so can only play a very limited role. The 5f shell of the actinides is more extended but, in the case of thorocene, lies high in energy and so can only provide modest stabilisation of the bond. In plutonocene, the 5f shell is energetically stabilised and can therefore contribute more substantially to the bond. This reasoning is supported by the structural data of Table 1, in which plutonocene exhibits the shortest ion-

Table 2 BCP properties of the M–C, C–C and C–H bonds in benzene, the COT dianion, and the metallocenes considered in this study. All values are given in a.u.

Property	C_6H_6	COT^{2-}	ThCOT2: $1\ ^1A_g$	PuCOT2: $1\ ^5A_g$	CeCOT2: $1\ ^1A_g$	CeCOT2: $2\ ^1A_g$
ρ_{M-C}	—	—	0.0421	0.0454	0.0395	0.0382
$\nabla^2\rho_{M-C}$	—	—	0.115	0.139	0.119	0.123
ρ_{C-C}	0.323	0.301	0.307	0.307	0.308	0.308
$\nabla^2\rho_{C-C}$	−0.969	−0.832	−0.860	−0.862	−0.868	−0.867
ρ_{C-H}	0.292	0.282	0.290	0.291	0.291	0.291
$\nabla^2\rho_{C-H}$	−1.13	−0.964	−1.10	−1.11	−1.11	−1.11

centroid separation. With respect to cerocene, the reduced separation is consistent with increased deviation from a purely electrostatic interaction, *i.e.* is indicative of increased covalent character in the Pu–C bonds.

The BCP data suggests that the 2 ^{1}Ag excited state of cerocene exhibits a slightly weaker bond than that of the 1 ^1A_g ground state. Again, this is to be expected. Considering again the CASSCF results presented here, the excited state is primarily comprised of configurations in which the '4f$_\delta$' orbital is occupied. Occupation of this orbital, which has anti-bonding character (see Fig. 2), would therefore be expected to weaken the metal–ligand interaction, as found here.

Both C–C and C–H bonds are, as expected, of clear covalent character. C–C BCPs show remarkable similarity in the metallocenes, and suggest C–C bonds that are marginally stronger than those of the COT dianion, but weaker than those of benzene. Metallocene C–H BCP data are extremely similar to those of benzene, and suggest slightly stronger C–H interactions than found in the COT dianion.

Finally, the reader's attention is drawn to the near identical C–C and C–H BCP data in the ground and excited states of cerocene, which suggest that the significant difference in configurational admixture between the two has little effect on the ligand electronic structure, presumably due to the strong metal–ligand hybridisation of the orbitals involved.

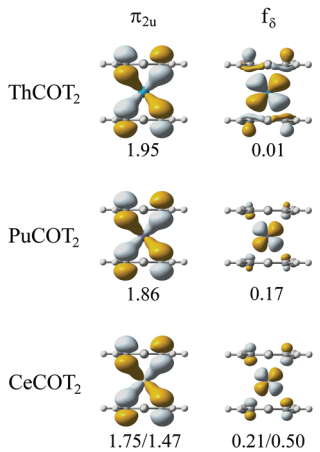

Fig. 2 Active space natural orbitals of a_u/b_{1u} symmetry, showing strong hybridisation between ligand π_{2u} and metal f_δ components.

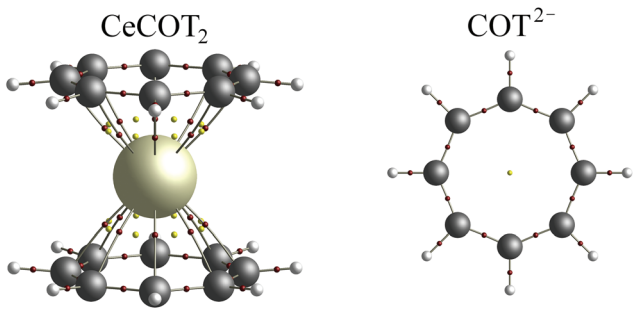

Fig. 3 QTAIM calculated molecular graphs of cerocene and the COT dianion. Nuclear critical points are overlayed with atoms, bond and ring critical points are indicated by red and yellow spheres, respectively.

QTAIM: integrated properties

While the topological analysis discussed in the previous section has proven useful in quantifying the difference in metal–ligand interactions in the complexes under study, as well as highlighting the similarities in the ligand electronic structure, the results suggest that there are only minor differences between the different electronic states of the metallocenes which form the focus of this study. In order to investigate the possibility of further differentiation, the one- and two-electron integrated properties that become available through QTAIM analysis are considered here. Integrating the electron density over an atomic basins Ω_i yields the electronic population of the atom, N_i, from which the atomic charge can be derived. If instead one takes the exchange-correlation component of the electron pair-density, then a pair of two-electron properties can be evaluated: the localisation index, λ_i, obtained by integration of both components of the pair density over the same atomic basin Ω_i, and the delocalisation index, δ_{ij}, obtained by integrating one component over Ω_i and one over Ω_j. λ_i corresponds to the average number of electrons localised upon a given atom, while δ_{ij} quantifies the average number of electrons shared between two atoms. Formally, the evaluation of these two-electron properties requires explicit knowledge of the 2nd order RDM. Construction of this matrix, however, is computationally demanding, and so approximate methods have been developed based on the 1st order RDM. In this work, the approximate form of the 2nd order RDM proposed by Müller[43] is employed.

Table 3 gives the integrated QTAIM properties associated with the M–C interactions of the metallocenes, calculated at the CASPT2-optimised geometries (results obtained at the B3LYP geometries can be found in Table S3 of the ESI†). Thorium has a significantly greater (~0.5 a.u.) positive charge than its lanthanide analogue Ce in the cerocene ground state. However, this alone cannot be taken as an indication of a difference in oxidation states between the two, since the Pu ion has a comparable charge to the latter (q_{Pu}–q_{Ce} = 0.042 a.u.).

Table 3 Integrated QTAIM properties associated with the metallocene M–C bond. N_i is the atomic population, q_i the atomic charge, λ_i the delocalisation index and δ_{ij} the delocalisation index. All values are given in a.u.

Property	ThCOT2: 1 ^1A_g	PuCOT2: 1 ^5A_g	CeCOT2: 1 ^1A_g	CeCOT2: 2 ^1A_g
N_M	87.454	91.984	56.026	56.051
q_M	+2.546	+2.016	+1.974	+1.949
λ_M	85.812	90.269	54.500	54.745
$Z_M - \lambda_M$	4.188	3.731	3.500	3.255
$N_M - \lambda_M$	1.642	1.715	1.526	1.306
N_C	6.135	6.103	6.099	6.097
q_C	−0.135	−0.103	−0.099	−0.097
λ_C	4.079	4.026	4.064	4.073
δ_{MC}	0.197	0.206	0.183	0.156

Table 4 Integrated QTAIM properties associated with the C–C and C–H bond in benzene, the COT dianion and metallocenes. All values are given in a.u.

Property	C_6H_6	COT^{2-}	ThCOT2: 1 ^1A_g	PuCOT2: 1 ^5A_g	CeCOT2: 1 ^1A_g	CeCOT2: 2 ^1A_g
N_C	5.968	6.191	6.135	6.103	6.099	6.097
q_C	+0.032	−0.191	−0.135	−0.103	−0.099	−0.097
λ_C	4.050	4.150	4.079	4.026	4.065	4.073
δ_{CC}	1.287	1.384	1.310	1.317	1.303	1.304
N_H	1.032	1.059	1.024	1.024	1.026	1.026
q_H	−0.032	−0.059	−0.024	−0.024	−0.026	−0.026
λ_H	0.476	0.485	0.460	0.459	0.461	0.461
δ_{CH}	0.987	0.986	0.973	0.970	0.974	0.975

Furthermore, in the excited 2 ^1A_g state of cerocene, which the CASSCF study performed here indicates is better characterised as a Ce(III) state, the Ce charge is very similar to that in the ground state.

Further information can be gained by considering the localisation indices. If the difference between λ_M and the atomic number, Z_M, of the metal ions is considered, it can be seen that Th has the smallest proportion of electrons localised on the metal centre, with 4.188 a.u. of electronic charge either shared between the metal and ligand, or transferred onto the ligand itself. In comparison, Pu shares/transfers a further 0.457 a.u., compared to an additional 0.688 a.u. in the cerocene ground state and 0.933 a.u. in the excited state. This trend correlates well with the increasing occupation of the anti-bonding 'f_δ' orbitals found in the natural orbital occupations analysis and further supports the interpretation of the cerocene 2 ^1A_g state as a Ce(III) state. The ground state, however, has a similar degree of electron sharing/transfer to that of plutonocene, supporting a Ce(IV) or mixed-valence interpretation.

Comparing the difference between the atomic population, N_M, and the localisation index gives an indication of the number of electrons shared by the ion in its interactions with the ligands (although it should be noted that there is also a contribution from electrons shared by the carbon atoms to this property). This is largest in plutonocene, whereas in the cerocene ground state the Ce ion shares a similar number of electrons as the Th ion in thorocene. In the cerocene excited state this value is reduced by 0.336 a.u. (0.220 a.u.) in comparison to the thorocene (cerocene) ground state. Combined, this data can be interpreted as clear evidence of increased covalent character in plutonocene when compared to thorocene and cerocene, supporting the presented structural evidence, and exhibiting the trend that would be expected based on the previous discussion of the contribution of the f-manifold to bonding. A similar trend is found in the metal–carbon delocalisation indices, δ_{MC}: again the greatest delocalisation is found in plutonocene, followed by thorocene and the ground and excited states of cerocene. Whilst the differences calculated here are small, it should be borne in mind that δ_{MC} measures the delocalisation between the ion and *each* ring carbon: summation gives the total number of electrons shared between the ion and COT rings as 3.296 in plutonocene, 3.152 in thorocene, and 2.928 (2.496) in the ground (excited) state of cerocene, again supporting the previous interpretation of the Ce oxidation states, and providing a clear quantifiable measure of covalency in these multiconfigurational complexes.

Similar analysis can be performed on the COT ring itself: Table 4 presents the relevant QTAIM data associated with the C–C and C–H bonds, calculated at the CASPT2-optimised geometries (results obtained at the B3LYP geometries can be found in Table S4 of the ESI†). Additionally, data for benzene and the charge-compensated COT dianion are presented. Carbon charges are very similar in all of the metallocenes and bear a closer resemblance to COT^{2-} than benzene, as might be expected considering their similar anionic character. $MCOT_2$ hydrogen charges are very similar to each other and to that of benzene. COT^{2-} hydrogen charges are slightly larger, indicating an increased diffusivity in the electron density, and explaining the slightly lower value of ρ_{C-H} in Table 2. Whilst C–C delocalisation indices are slightly larger in the metallocenes than in benzene, they are smaller than in COT^{2-}, indicating marginally less electron sharing amongst the ring carbons in the ligated COT ring. More important though, is the similarity in δ_{CC} for all the metallocenes. If the difference between a trivalent and tetravalent oxidation state was the occupation of an additional localised f orbital, a significant difference between the C–C delocalisation indices would be expected, due to one less delocalised π-electron on the COT ligand. The calculations performed here indicate that a localised 4f electron is not present in either the ground or excited ^1A_g states $CeCOT_2$, but the mixed-valence character of the former would be expected to result in some difference in the ligand C–C bonding. While a difference is indeed found, it is very slight. Even summing over the eight ligand carbons, the reduction in the number of electrons shared in the ring is 0.112 when compared to plutonocene, and just 0.056 when compared to thorocene. Furthermore, it might be expected that the difference in configurational admixture between the ground and excited ^1A_g states of cerocene would manifest itself in some difference in the ligand electronic structure, particularly with respect to its aromaticity. However, the delocalisation indices are, again, almost identical. The difference between the ground and excited states of cerocene is considered in Fig. 4, which shows density-difference plots, ρ_{GS}–ρ_{ES}. The first pair of isosurfaces in pane 4(a) show that the ground state has greater electronic charge on the outside of the COT ring and in a diffuse region around the Ce ion, whereas the excited state has increased charge on the inside of the ring and in a more

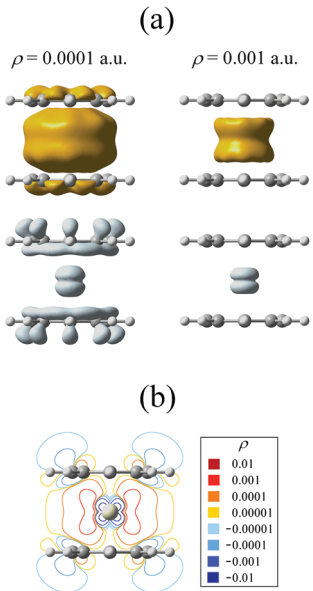

Fig. 4 (a) Density difference plots highlighting the difference between the ground and excited ^1A_g states of cerocene. Gold isosurfaces correspond to positive electron density, blue to negative density. (b) Contour plot of the same property, evaluated in the *yz*-plane containing the Ce ion.

localised region around the ion. These isosurfaces, however, correspond to a low value of electron density (10^{-4} a.u.). Increasing the value of the isosurface to 0.001 a.u reveals that the major difference between the two states is a contraction of the Ce density in the excited state, with little variation in the ring density, thus explaining the similar QTAIM δ_{CC} data discussed above.

f-Electron populations and orbitally resolved localisation indices

Within the Hartree–Fock approximation, atomic electron populations, as well as (de)localisation indices, can be decomposed into contributions from the set of occupied molecular orbitals.[44,45] Assuming the Müller approximation to the 2nd order RDM[43] allows an analogous approach to be taken at the CASSCF level of theory. Here, contributions from active space orbitals exhibiting π_{2u} and 4f(Ce)/5f(Th,Pu) character are considered, allowing a quantitative measure of f-electron density and localisation in these complexes. Table 5 reveals a significant difference in f_δ occupation between thorocene and all other complexes. Both plutonocene and cerocene exhibit populations close to 1, with the cerocene excited state population being 1.053, presumably due to a weak divalent contribution to the configurational admixture. The f_δ population in the ground state of cerocene of 0.949 is in good agreement with both the experimental value[10] of 0.89 ± 0.03 and the theoretical value of 0.90 ± 0.04 obtained previously.[13]

Table 5 Orbitally resolved atomic populations, N^{OR}, and localisation indices, λ^{OR}. Only active space orbitals exhibiting π_{2u} and f_δ character are considered. All values are in a.u.

System	$N^{OR}_{f_\delta}$	λ^{OR}_{M}
$ThCOT_2$ ^1A_g	0.293	0.050
$PuCOT_2$ ^5A_g	0.933	0.615
$CeCOT_2$ 1 ^1A_g	0.949	0.704
$CeCOT_2$ 2 ^1A_g	1.053	0.990

Consideration of the orbitally resolved localisation indices again reveal a significant difference between thorocene and all other complexes: whilst thorocene exhibits only negligible f_δ localisation, plutonocene and the ground state of cerocene show similar and substantial degrees of localisation, 0.615 and 0.704 respectively, again supporting a mixed-valence interpretation. The cerocene excited state has an f_δ localisation index of 0.99, in accordance with a trivalent oxidation state.

Summary and conclusions

The electronic structures of thorocene, plutonocene and cerocene have been calculated at the CASSCF level of theory. Analysis of the natural orbitals shows that while thorocene is well characterised in terms of a single configuration, both plutonocene and cerocene exhibit significant multiconfigurational character. In terms of natural orbital occupancies, plutonocene bears a striking resemblance to cerocene. When considering configurational admixture, the ground state of cerocene is best described as mixed valence, whilst the first excited state of ^1A_g symmetry is better described as a Ce(III) state. Closer inspection of the natural orbitals reveals strong hybridisation of the ring π_{2u} and metal f_δ orbitals, this being most pronounced in cerocene. Since the combination of multiconfigurational character and orbital hybridisation makes further analysis difficult, QTAIM has been applied to order to provide an unambiguous analysis of the electronic structure of these complexes. QTAIM clearly and quantitatively reveals that plutonocene exhibits the most covalent metal–ligand interaction, supporting the structural data showing that the ion-centroid separation in this complex is significantly smaller than in cerocene. The excited state of cerocene is found to exhibit a weaker ring–metal interaction, commensurate with the increased occupation of the anti-bonding 'f_δ' orbital. QTAIM also reveals that cerocene exhibits a higher proportion of electronic charge associated with the central ion than thorocene which might, at first glance, be taken as evidence of a Ce(III) state. Plutonocene, however, also exhibits the same behaviour, suggesting that this is in fact due to the multiconfigurational character of these complexes.

When considering the degree of electron sharing/transfer in the metallocenes, it is found that this is most pronounced in the excited state of cerocene, strongly supporting the assignment of a Ce(III) excited state. Plutonocene, along with the ground state of cerocene, shows significantly greater electron sharing/transfer than that found in thorocene. Whilst this is slightly more pronounced in cerocene, it is insufficient to support a Ce(III) oxidation state. Further analysis reveals that the average number of electrons shared by the Pu ion is greater than that of Th or Ce, quantifiable evidence of greater

covalent character in plutonocene. The degree of electron sharing by the ion is similar for Th and Ce in the cerocene ground state (although slightly greater in the former), whereas the excited state shows a significant reduction in electron sharing, again commensurate with increased occupation of the anti-bonding 'f_δ' orbital. The total number of electrons shared between the metal and ligand is significantly lower in the excited state of cerocene, supporting a Ce(III) assignment. Whilst the cerocene ground state exhibits reduced electron sharing, this is not sufficiently pronounced to conclude anything other than a Ce(IV) or mixed-valence assignment. These assignments are further supported by data obtained from the orbital decomposition of atomic populations and localisation indices.

QTAIM analysis of the ring C–C bonds show remarkable similarity between the metallocenes, suggesting that changes in electron density at the metal centre, as exhibited in the ground and excited ^1A_g states of cerocene, have only a small effect on the ligand, presumably due to the strong hybridisation of the π_{2u} and f_δ orbitals. Consideration of the C–C delocalisation indices, which indicate the degree of electron sharing in the ligand, and can be related to its aromaticity, suggest that the ligand π-systems in all metallocenes bear a strong resemblance to the archetypal aromatic system benzene and the COT dianion implying that, even if there are differences in formal oxidation state, the aforementioned strong hybridisation results in a largely unchanged ligand electronic structure.

In summary, all methods of analysis support the conclusion that cerocene is best described as Ce(IV) or mixed-valence complex in which the strong metal–ligand hybridisation and higher degree of electron delocalisation results in accumulation of charge on the Ce centre. As has been shown, the ligand electronic structure in the ground and excited states of cerocene is very similar, even though the latter would be best classified as a Ce(III) state. Measures of the effective oxidation state might therefore be expected to give results comparable to those of formal Ce(III). A similar conclusion has been reached previously.[13] It would be interesting to perform XANES measurements on the formally tetravalent plutonocene, which has been shown here to bear a strong similarity to cerocene: experimentally, both complexes have been shown to exhibit temperature independent paramagnetism (TIP),[10,46] although its origin differs between the two.

Finally, the combination of CASSCF electronic structure calculations and QTAIM topological analysis has been shown to be extremely useful in order to probe details of electronic structure that are difficult to analyse using traditional methods when strong hybridisation and multiconfigurational character are present. The results presented here demonstrate, in a quantifiable manner, that plutonocene exhibits larger metal–ligand covalency than thorocene, whilst such covalent character is weakest in cerocene. This is what might be expected for these systems, but the ability to quantitatively assess such properties has important implications, particularly with regard to problems in the separation of lanthanides from minor actinides in spent nuclear fuel, where the increased covalency of the latter is the mechanism believed to be responsible for the selectivity of soft-donor ligands.

Acknowledgements

The author would like to thank the EPSRC for the award of a career acceleration fellowship (grant EP/J002208/1), UCL research computing for access to the Legion and Unity HPC facilities, the National Service for Computational Chemistry Software (NSCCS) for access to the Columbus HPC facility and the support of the Thomas Young Centre for the theory and simulation of materials.

References

1 M. L. Neidig, D. L. Clark and R. L. Martin, *Coord. Chem. Rev.*, 2013, **257**, 394–406.
2 N. Kaltsoyannis, *Inorg. Chem.*, 2013, **52**, 3407–3413.
3 M. P. Jensen and A. H. Bond, *J. Am. Chem. Soc.*, 2002, **124**, 9870–9877.
4 H. H. Dam, D. N. Reinhoudt and W. Verboom, *Chem. Soc. Rev.*, 2007, **36**, 367–377.
5 F. Lewis, M. Hudson and L. Harwood, *Synlett*, 2011, 2609–2632.
6 A. Greco, S. Cesca and G. Bertolini, *J. Organomet. Chem.*, 1976, **113**, 321–330.
7 A. Streitwieser, S. A. Kinsley, J. T. Rigsbee, I. L. Fragala, E. Ciliberto and N. Rosch, *J. Am. Chem. Soc.*, 1985, **107**, 7786–7788.
8 K. N. Raymond and C. W. Eigenbrot, *Acc. Chem. Res.*, 1980, **13**, 276–283.
9 A. Streitwieser, S. A. Kinsley, C. H. Jenson and J. T. Rigsbee, *Organometallics*, 2004, **23**, 5169–5175.
10 C. Booth, M. Walter, M. Daniel, W. Lukens and R. Andersen, *Phys. Rev. Lett.*, 2005, **95**, 267202.
11 N. M. Edelstein, P. G. Allen, J. J. Bucher, D. K. Shuh, C. D. Sofield, N. Kaltsoyannis, G. H. Maunder, M. R. Russo and A. Sella, *J. Am. Chem. Soc.*, 1996, **7863**, 13115–13116.
12 M. Dolg, P. Fulde, W. Küchle, C.-S. Neumann and H. Stoll, *J. Chem. Phys.*, 1991, **94**, 3011.
13 A. Kerridge, R. Coates and N. Kaltsoyannis, *J. Phys. Chem. A*, 2009, **113**, 2896–2905.
14 A. Kerridge and N. Kaltsoyannis, *C. R. Chim.*, 2010, **13**, 853–859.
15 R. Coates, M. Coreno, M. DeSimone, J. C. Green, N. Kaltsoyannis, A. Kerridge, N. Narband and A. Sella, *Dalton Trans.*, 2009, 5832–5840.
16 M. Dolg, P. Fulde, H. Stoll, H. Preuss, A. Chang and R. M. Pitzer, *Chem. Phys.*, 1995, **195**, 71–82.
17 A. Kerridge and N. Kaltsoyannis, *J. Phys. Chem. A*, 2009, **113**, 8737–8745.
18 J. C. Marra, A. D. Cozzi, R. A. Pierce, J. M. Pareizs, A. R. Jurgensen and D. M. Missimer, in *Environmental*

Issues and Waste Management Technologies in the Ceramic and Nuclear Industries VI, ed. G. L. Smith, S. K. Sundaram and D. R. Spearing, John Wiley and Sons, Chichester, 2012, pp. 381–404.
19 P. Löwdin, *Phys. Rev.*, 1955, **376**, 1474–1489.
20 R. F. W. Bader, *Atoms in Molecules: A Quantum Theory*, Oxford University Press, Oxford, 1990.
21 B. Roos, P. R. Taylor and P. E. M. Siegbahn, *Chem. Phys.*, 1980, **48**, 157–173.
22 G. Karlström, R. Lindh, P.-Å. Malmqvist, B. O. Roos, U. Ryde, V. Veryazov, P.-O. Widmark, M. Cossi, B. Schimmelpfennig, P. Neogrady and L. Seijo, *Comput. Mater. Sci.*, 2003, **28**, 222–239.
23 F. Aquilante, L. D. E. Vico, N. Ferré, G. Ghigo, P.-Å. Malmqvist, P. Neogrády, T. B. Pedersen, M. P. Nák, M. Reiher, B. O. Roos, L. Serrano-andrés, M. Urban, V. Veryazov and R. Lindh, *J. Comput. Chem.*, 2010, **31**, 224–247.
24 B. O. Roos, R. Lindh, P.-Å. Malmqvist, V. Veryazov and P.-O. Widmark, *J. Phys. Chem. A*, 2004, **108**, 2851–2858.
25 B. O. Roos, R. Lindh, P.-A. Malmqvist, V. Veryazov, P.-O. Widmark and A. C. Borin, *J. Phys. Chem. A*, 2008, **112**, 11431–11435.
26 B. O. Roos, R. Lindh, P.-Å. Malmqvist, V. Veryazov and P.-O. Widmark, *Chem. Phys. Lett.*, 2005, **409**, 295–299.
27 K. Anderson, P.-Å. Malmqvist, B. O. Roos, A. J. Sadlej and K. Wolinskit, *J. Phys. Chem.*, 1990, 5483–5488.
28 P. Hohenberg and W. Kohn, *Phys. Rev.*, 1964, **155**, B864–B871.
29 W. Kohn and L. J. Sham, *Phys. Rev.*, 1965, **140**, A1133–A1138.
30 A. D. Becke, *J. Chem. Phys.*, 1993, **98**, 5648.
31 P. Stephens, F. Devlin, C. Chabalowski and M. Frisch, *J. Phys. Chem.*, 1994, **98**, 11623–11627.
32 R. Ahlrichs, M. Bär, M. Häser, H. Horn and C. Kölmel, *Chem. Phys. Lett.*, 1989, **162**, 165–169.
33 F. Weigend and R. Ahlrichs, *Phys. Chem. Chem. Phys.*, 2005, **7**, 3297–3305.
34 X. Cao and M. Dolg, *J. Chem. Phys.*, 2001, **115**, 7348.
35 W. Küchle, M. Dolg, H. Stoll and H. Preuss, *J. Chem. Phys.*, 1994, **100**, 7535.
36 T. A. Keith, *AIMAll (Version 13.05.06)*, TK Gristmill Software, Overland Park, KS, USA, 2013.
37 T. Lu and F. Chen, *J. Comput. Chem.*, 2012, **33**, 580–592.
38 A. Avdeef, K. N. Raymond, K. O. Hodgson and A. Zalkin, *Inorg. Chem.*, 1972, **11**, 1083–1088.
39 M. W. Schmidt and M. S. Gordon, *Annu. Rev. Phys. Chem.*, 1998, **49**, 233–266.
40 I. Kirker and N. Kaltsoyannis, *Dalton Trans.*, 2011, **40**, 124–131.
41 M. Tassell and N. Kaltsoyannis, *Dalton Trans.*, 2010, **39**, 6576–6588.
42 R. F. W. Bader and C. F. Matta, *Found. Chem.*, 2012, 1–24.
43 A. M. K. Müller, *Phys. Lett. A*, 1984, **105**, 446–452.
44 R. F. W. Bader and M. E. Stephens, *J. Am. Chem. Soc.*, 1975, **97**, 7391–7399.
45 X. Fradera, M. A. Austen and R. F. W. Bader, *J. Phys. Chem. A*, 1999, **103**, 304–314.
46 D. C. Eisenberg, A. Streitwieser and W. K. Kot, *Inorg. Chem.*, 1990, **29**, 10–14.